Chemical Engineering Journal 155 (2009) 931–940

Contents lists available at ScienceDirect

Chemical Engineering Journal

journal homepage: www.elsevier.com/locate/cej

Influence of the activation conditions on the porosity development of herringbone carbon nanofibers

Vicente Jiménez [b,*], José Antonio Díaz [b], Paula Sánchez [b], José Luis Valverde [b], Amaya Romero [a]

[a] Facultad de Ciencias Químicas/Escuela Técnica Agrícola, Universidad de Castilla-La Mancha, 13071 Ciudad Real, Spain
[b] Facultad de Ciencias Químicas/Departamento de Ingeniería Química, Universidad de Castilla-La Mancha, 13071 Ciudad Real, Spain

ARTICLE INFO

Article history:
Received 24 June 2009
Received in revised form
16 September 2009
Accepted 19 September 2009

Keywords:
Carbon nanofibers
Activation
Porosity
Carbon yield
Adsorption

ABSTRACT

The influence of different activation conditions, including activating agent/CNFs mass ratio, activation temperature, activation time and He flow rate, on the pore structure development of herringbone carbon nanofibers (CNFs) has been studied. Activation conditions with a KOH/CNFs mass ratio = 5/1, activation temperature = 850 °C, activation time = 3 h and He flow rate = 700 mL min^{-1} gave rise to a material with a very high micropore volume, a quite narrow micropore distribution and the highest surface area (increased by a factor of 4.5 in comparison to the raw CNFs). The conditions outlined above also led to the creation of some mesopores in the activation process due to the strong interaction between the CNFs and the activating agent. On the other hand, the use of other activation conditions led to activated CNFs with different structural properties. For example, activated CNFs with the lowest mesopore volume were obtained when the activation conditions were KOH/CNFs mass ratio = 5/1, activation temperature = 900 °C, activation time = 3 h and He flow rate = 500 mL min^{-1}. Therefore, depending on the final application of the activated CNFs, it is possible to control their pore structure by selecting appropriate activation conditions.

1. Introduction

Carbon nanofibers (CNFs) represent one of the most promising materials for many applications such as catalytic support [1], polymer reinforcement agents [2], fuel cell electrodes [3], adsorbents [4] and hydrogen storage [5] amongst others. In many cases, the problem associated with these structures is that their specific surface area is not very high (typical value around 200 m^2/g), a situation that is detrimental for many applications such as those regarding gas and energy storage, both of which are strongly dependent on the remarkable surface and structural properties of such materials.

In this regard, the porosity properties of carbons can be significantly modified by activation processes that remove the most reactive carbon atoms from their structure. There are essentially two different processes for the preparation of activated carbons, the so-called *physical* and *chemical* activation approaches. The first process involves carbonisation of a precursor followed by controlled gasification of the carbonised material and then direct activation of the starting material in the presence of an activating agent such as CO_2 or steam (or a combination of the two). In the chemical activation process, the parent carbon material is mixed with an activating agent (e.g. KOH, NaOH, $ZnCl_2$) and this is followed by pyrolysis [6,7].

Chemical activation has been shown to be a very efficient method to obtain carbons with high surface area and narrow micropore distribution. The most important advantage of chemical activation over physical activation is that the sample is activated at a lower temperature. Other advantages are that higher yields and greater porosity development are obtained and less time is required for the activation process. Key disadvantages of the chemical activation process are the need for a thorough washing step due to the incorporation of impurities arising from the activating agent, which may affect the final chemical properties of the activated carbon [8] and the corrosiveness of the process [6].

The recent literature contains many examples of the chemical activation of carbon using alkali hydroxide (mainly KOH and NaOH) [9–11]. Nevertheless, very few of these studies focused on CNFs and, more specifically, on the study of the influence of the activation conditions on their porous texture development [12–15]. In this regard, the activation of materials with ordered graphitic structure (such as CNFs) is more difficult than the activation of amorphous carbon [16,17]. Furthermore, the type of carbon nanofibers, i.e. herringbone, ribbon or platelet [12,18], can also influence the pore properties of the final activated material.

Despite the fact that although the activation of carbon materials is a common and frequently used process, its mechanism is not well understood and the various interpretations that can be found in literature underline the complexity of the process [11,19,20]. In general terms, chemical activation by hydroxides consists of

* Corresponding author. Tel.: +34 926295300; fax: +34 926295318.
E-mail address: vicente.jimenez@uclm.es (V. Jiménez).

1385-8947/$ – see front matter © 2009 Elsevier B.V. All rights reserved.
doi:10.1016/j.cej.2009.09.035

Table 1
Textural properties and other characterization parameters of raw and activated CNFs by using KOH as the activating agent.

KOH/CNFs mass ratio	Temperature (°C)	Time (h)	He flow rate (mL min^{-1})[a]	Carbon yield (%)	BET surface area (m^2/g)	Micropore area (m^2/g)[b]	Micropore volume (cm^3/g)[c]	Mesopore volume (cm^3/g)[d]	npg[e]	TPO temperature range (°C)[f]	Range CNFs diameter[g]	C (mol%)	H (mol%)	O (mol%)[h]	C/O
Parent CNFs					127.2	33.2 (26%)	0.147 (20%)	0.590	10.8	448–580 (538)	5–160	92.0	5.5	2.5	37.3
1/1	850	3	500	90.4	161.3	72.3 (45%)	0.396 (45%)	0.472	10.7	398–520 (498)	25–160	89.1	5.5	5.5	16.3
2/1	850	3	500	80.5	251.8	127.9 (51%)	1.110 (69%)	0.486	9.7	372–500 (472)	25–155	87.5	5.0	7.5	11.7
3/1	850	3	500	70.9	334.9	153.5 (46%)	1.898 (80%)	0.479	8.9	361–530 (469)	15–90	83.7	5.0	11.4	7.4
4/1	850	3	500	55.1	407.5	173.0 (42%)	2.361 (74%)	0.806	8.2	330–500 (435)	10–80	80.0	5.0	15.0	5.3
5/1	850	3	500	42.3	433.0	229.1 (53%)	3.137 (83%)	0.633	7.9	317–497 (424)	15–75	78.7	4.6	16.7	4.7
6/1	850	3	500	50.5	414.0	210.0 (51%)	2.867 (81%)	0.669	8.1	325–510 (427)	30–80	79.9	5.0	15.1	5.3
5/1	700	3	500	84.6	226.0	100.1 (44%)	0.954 (66%)	0.498	9.7	382–520 (477)	25–160	88.7	5.0	6.3	14.0
5/1	800	3	500	66.1	369.5	148.9 (41%)	2.748 (81%)	0.650	8.8	340–498 (432)	25–100	81.9	4.7	13.4	6.1
5/1	850	3	500	42.3	433.0	229.1 (53%)	3.137 (83%)	0.633	7.9	317–497 (424)	15–75	78.7	4.6	16.7	4.7
5/1	900	3	500	65.8	378.5	231.1 (61%)	3.486 (93%)	0.272	8.7	334–502 (437)	25–85	81.1	4.9	14.0	5.8
5/1	850	1	500	66	364.7	159.0 (44%)	2.315 (80%)	0.603	8.8	359–511 (449)	25–140	82.7	5.0	12.2	6.8
5/1	850	2	500	52.6	409.5	208.9 (51%)	2.875 (82%)	0.614	8.3	325–484 (437)	20–110	80.0	4.6	15.4	5.2
5/1	850	3	500	42.3	433.0	229.1 (53%)	3.137 (83%)	0.633	7.9	317–497 (424)	15–75	78.7	4.6	16.7	4.7
5/1	850	4	500	45.1	431.7	205.6 (49%)	2.683 (77%)	0.786	7.9	329–494 (432)	20–100	78.9	5.0	16.1	4.9
5/1	850	3	150	74.2	320.3	113.8 (36%)	1.860 (73%)	0.689	9	366–515 (466)	10–110	83.9	5.0	11.1	7.6
5/1	850	3	500	42.3	433.0	229.1 (53%)	3.137 (83%)	0.633	7.9	317–497 (424)	15–75	78.7	4.6	16.7	4.7
5/1	850	3	700	20.1	569.9	305.0 (54%)	3.431 (75%)	1.149	6.7	290–490 (390)	5–75	73.1	4.6	22.3	3.3
5/1	850	3	850	30.3	537.7	244.3 (45%)	3.226 (77%)	0.986	7	307–507 (410)	10–80	74.9	4.7	20.4	3.7
5/1	850	3	1000	46.2	431.2	207.3 (48%)	2.344 (76%)	0.743	7.9	320–510 (428)	25–110	79.1	5.0	15.9	5.0

[a] He flow rate measurement to 25 °C and 1 bar.
[b] In brackets: percentage of micropore area with respect to the total surface area.
[c] Cumulative micropore volume obtained using the Horvath–Kawazoe method. In brackets: percentage of micropore volume with respect to the total pore volume.
[d] Cumulative mesopore volume obtained using the BJH method.
[e] Number of graphene planes in the crystallites (npg = Lc/d_{002})
[f] In brackets: temperature at which the maximum of the oxidation temperature peak appears.
[g] Range CNFs diameter determined by counting ~200 CNFs on the TEM images.
[h] O_{diff}: the oxygen is assessed by difference up to 100%.

solid–solid or solid–liquid reactions involving hydroxide reduction and carbon oxidation to generate porosity [15,20–22].

Although a wide variety of carbon precursors have been activated by alkaline hydroxides [23,24] (e.g. coals, polymers, lignocellulosic materials), a very limited number of reports in the literature concern the activation of carbon nanofibers by hydroxides [7,12,13]. Moreover, it is also very important to investigate the influence of different activation conditions on the final porous texture of these materials. In previous works [16,17], we studied the influence of the metal cation in the hydroxide and the type of gas used as the protector (He, Ar or N_2) during the process. It was found that He was the best protector gas; KOH and RbOH were the best activating agents.

In the work described here, we studied the influence of the most important operating conditions on the activation of carbon nanofibers: KOH/CNFs mass ratio, activation temperature, activation time and helium flow rate. A range of different characterization techniques were used to evaluate the structural changes in the activated CNFs: N_2 adsorption–desorption, XRD, TPO, TEM and elemental composition analysis.

2. Experimental

2.1. Preparation of CNFs

Carbon nanofibers (herringbone type) were grown at atmospheric pressure in a fixed-bed reactor (quartz tube of 2.5 cm diameter and 75 cm length) located in a vertical oven at a temperature of 600 °C. In each synthesis run, 100 mg of the prepared catalyst (Ni/SiO_2) was placed in the centre of the reactor and activated by heating (10 °C min^{-1}) in a flow of dry 20% (v/v) H_2/He (100 mL min^{-1}) at the desired reaction temperature (600 °C). The reduced activated catalyst was thoroughly flushed with dry He (100 mL min^{-1}) for 1 h before introducing the C_2H_4/H_2 (4%, v/v) feed. The growth time was 1 h. Silica supports were subsequently separated from the carbon product by leaching the primary product in hydrofluoridic acid (70%) for 15 h under vigorous stirring followed by filtration and washing [8,24,25].

2.2. CNFs activation

The experimental setup used for the preparation of activated CNFs consisted of a horizontal quartz reactor tube with a conventional horizontal furnace. CNFs were chemically activated using KOH as an activating agent. As a representative example, CNFs (1.5 g) were mixed with the corresponding activating agent and distilled water (10 mL water for 2 g activating agent). The mixture was heated at 85 °C for 4 h with stirring and then dried for 12 h at 110 °C. The activating KOH/CNFs mixture was then placed on a ceramic crucible located inside a horizontal reactor tube. The heat treatment consisted of a heating ramp from ambient temperature to the final heat treatment temperature at a heating rate of 5 °C min^{-1}, followed by a plateau of 1, 2, 3 or 4 h under a set helium flow rate. The system was then cooled back to the initial temperature [6,12,13]. The activated product was first washed with hydrochloric acid (5 M) to remove the activating agent and then with distilled water until a neutral washing was obtained. The resulting material was dried for 12 h at 110 °C in air to remove water prior to characterization [6,14].

2.3. Characterization of CNFs

Surface area/porosity measurements were carried out using a Micromeritics ASAP 2010 sorptometer apparatus with N_2 at 77 K as the sorbate. The samples were outgassed at 453 K under vacuum (6.6×10^{-9} bar) for 16 h prior to analysis; specific surface areas were determined by the multipoint BET method, pore geometry and size distributions were evaluated using the standard BJH treatment and micropore size distribution was evaluated using the Horvath–Kawazoe (H–K) equation.

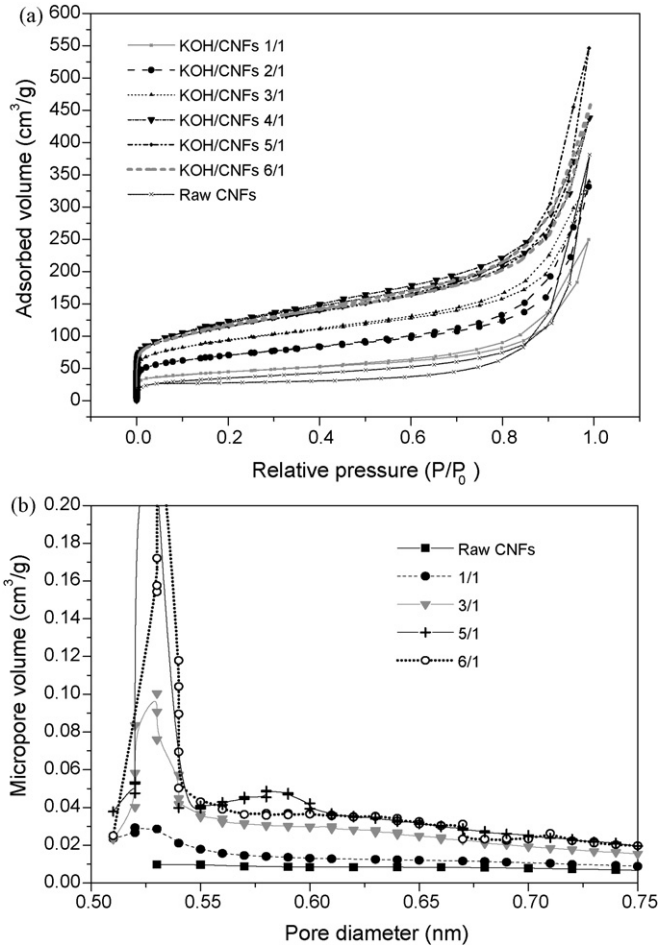

Fig. 1. *Influence of the KOH/CNFs ratio*: (a) N_2 adsorption–desorption isotherms and (b) micropore size distribution.

XRD analyses were carried out on a Philips X'Pert instrument using nickel filtered Cu-Kα radiation; the samples were scanned at a rate of 0.02° step^{-1} over the range $5° \leq 2\theta \leq 90°$ (scan time = 2 s step^{-1}).

The elemental composition of the carbon nanofibers was determined using a LECO elemental analyzer (model CHNS-932), which had an IR analyzer for carbon, hydrogen and sulphur and a TCD analyzer for nitrogen. Oxygen was assessed by difference.

Diameter distribution and the morphology of the carbon nanofibers were probed by transmission electron microscopy (TEM) using a Philips Tecnai 20T, operated at an acceleration voltage of 200 keV. Suitable specimens were prepared by ultrasonic dispersion in acetone with a drop of the resultant suspension evaporated onto a holey carbon supported grid. The diameter distribution was measured by counting ~200 CNFs on the TEM images.

Temperature-programmed oxidation (TPO) was used to determine the crystallinity of the carbon nanofibers. The analyses were performed on 50 mg samples using a Micromeritics AutoChem 2950 HP apparatus with a flow of 50 mL min^{-1} of 20% (v/v) O_2/He mixture and a heating rate of 5 °C min^{-1} up to 1000 °C.

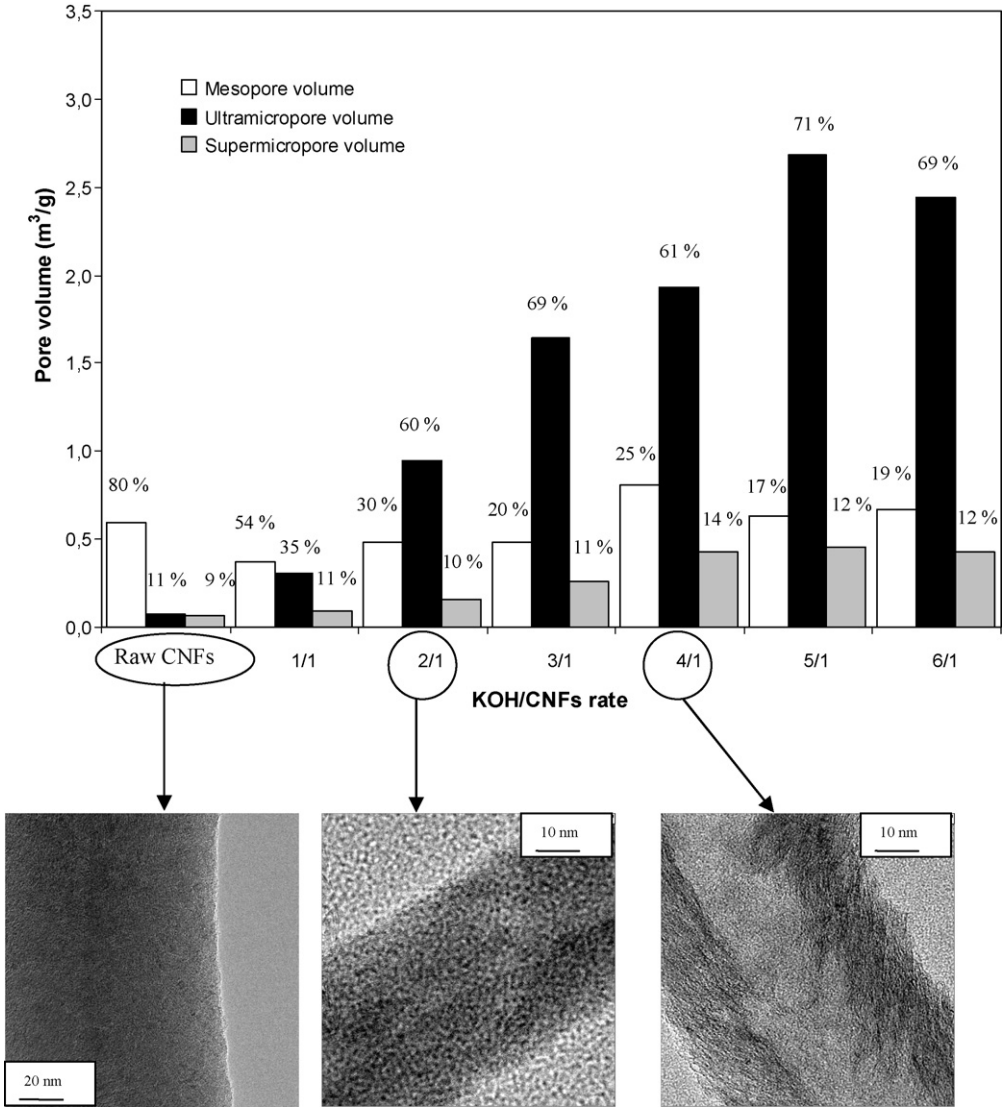

Fig. 2. *Influence of the KOH/CNFs ratio*: proportion of ultramicropores, supermicropores and mesopores. Representative TEM images.

3. Results and discussion

The strategy to maximize textural properties involved stepwise changes in different parameters such as the KOH/CNFs mass ratio, pyrolysis temperature, pyrolysis time and helium flow rate (measurement to 25 °C and 1 bar). The activation conditions that were studied in detail are summarized in Table 1. All of these parameters had a significant effect on the final pore characteristics of the activated CNFs.

3.1. Influence of the KOH/CNFs ratio

In order to investigate the influence of the KOH/CNFs mass ratio on the final properties of the activated material, the ratio was varied in the range 1/1–6/1 while keeping the other parameters constant (He flow rate, activation temperature and activation time were maintained at 500 mL min^{-1}, 850 °C and 3 h, respectively).

The porous texture characterization results for the activated samples are given in Table 1. The BET surface area was, in all cases, significantly larger than that of the parent CNFs, thus showing the important effect that the treatment has on the porosity of carbon nanostructures. It can be seen that both the BET surface area and the micropore volume increased continuously with the KOH/CNFs mass ratio, reaching a maximum for a value of 5/1. At higher values (6/1) the microporosity did not increase further [6]. As far as the mesopore development is concerned, this only took place to a significant extent at KOH/CNFs mass ratio values up to 4/1. It is remarkable to note that the micropore volume percentages (with respect to the total pore volume) of all activated samples increased, after the activation process, up to a KOH/CNFs mass ratio of 4/1.

The nitrogen isotherms measured at 77 K for different activated CNFs are shown in Fig. 1a. All the isotherms correspond to a mixture of types I–IV (according to the IUPAC classification) associated with both micropores and mesopores, with a hysteresis loop resulting from capillary condensation in the mesopores. It can be observed that once the micropores were filled at low relative pressure ($P/P_0 < 0.03$), the adsorption became significant on the non-microporous surface to be characterized by the slope at higher relative pressures. Thus, both the microporous and mesoporous domains increased with increasing KOH/CNFs mass ratio [12]. The activated CNFs micropore size distribution analyzed by the Howard-Kawazoe (H–K) method is represented in Fig. 1b. Clear differences can be seen between CNFs activated using different KOH/CNFs mass ratios.

The proportions of ultramicropores, supermicropores and mesopores in the activated samples are shown in Fig. 2. The

following classification of the pores (IUPAC) was considered: micropore < 2 nm (supermicropore: 0.7–2 nm and ultramicropores: <0.7 nm); 2 nm < mesopore < 50 nm and macropore > 50 nm. It can be seen that an increase in the amount of KOH in the activation process produced a linear rise in the ultramicropore volume (coincident with the BET surface area increase) of the activated materials, reaching a maximum value when the KOH/CNFs mass ratio was 5/1. Moreover, some supermicropores and mesopores were also generated, the latter only with high levels of KOH (KOH/CNFs mass ratio values of 4/1). The total mesopore volume decrease observed in activated materials (KOH/CNFs mass ratio values < 4/1) compared to that of the raw material is the result of the interaction between the initial mesopores (inherent to raw CNFs) and the chemical agent responsible for the activation process (K) generating new micropores [26]. In all cases the percentage of mesoporosity inherent in the parent CNFs decreased during the activation process due to large amount of ultramicropores created. Based on these results, it is possible depending on the KOH/CNFs mass ratio used in the activation process to control the pore size (ultramicropores, supermicropores or mesopores) of the resulting activated CNFs. Thus, it is possible to develop only micropores while maintaining a constant mesopore level (KOH/CNFs mass ratio values > 4/1), decreasing the mesopores (KOH/CNFs mass ratio values < 4/1) or increasing both micropores and mesopores (KOH/CNFs mass ratio values = 4/1).

These results suggest that, in the pore development, there were different pore opening mechanisms operating in CNFs activated using different KOH/CNFs mass ratios. While the micropore development in CNFs can be correlated with the partial opening of graphite layers (KOH/CNFs mass ratio values = 4/1), the mesopore development is probably related to other phenomena such as breaking of nanofibers or full exfoliation of graphite layers, which can led to different sizes of mesopores depending on the extent of the exfoliation process and can even result in the collapse of some micropore structures [13]. This fact was verified by examination of the TEM pictures in Fig. 2, in which a long but discontinuous hollow core is clearly visible along the fiber length at KOH/CNFs = 4/1 due to exfoliation. New mesopores were not generated when the KOH/CNFs mass ratio reached a value of 5/1 and, in fact, some even disappeared, a phenomenon attributed to their interaction with excess activating agent to generate new micropores [26].

As expected, the yield of CNFs was inversely proportional to the BET surface area variation because, during the activation process, the most reactive carbon atoms were removed from the raw structure thus increasing the surface area of the resulting material.

X-ray diffraction was used to study the graphitic character of the activated materials. The interpretation of the peak indexation of CNFs is sometimes complicated due to their unique structure (turbostratic nature, curvature, CNFs size, etc.), which may induce peak broadening and eventually peak shift [27]. All samples showed a peak near 26° and another one at around 45°, corresponding to hexagonal and rhombohedral graphite, respectively [28,29]. These peaks became sharper for lower KOH/CNFs mass ratio values, indicating that these CNFs were more graphitic than those activated with higher KOH/CNFs values when compared with the parent CNFs. Nevertheless, since the activated samples had different diameters (the diameter range shown in Table 1 indicates a narrower distribution on increasing the pore development), the changes in the X-ray patterns are due not only to changes in the structural order but also to changes in the CNFs sizes. For this reason, to ensure that changes in XRD peaks were due to changes in the structural order of the CNFs, the degree of graphitization was also measured by means of TPO analyses carried out under an O_2 environment. During the activation process the graphitic structure of the CNFs was, in part, destroyed, generating structural defects in their structure. Thus, highly activated CNFs may be oxidized at lower temperatures and over a wider temperature range (Table 1)

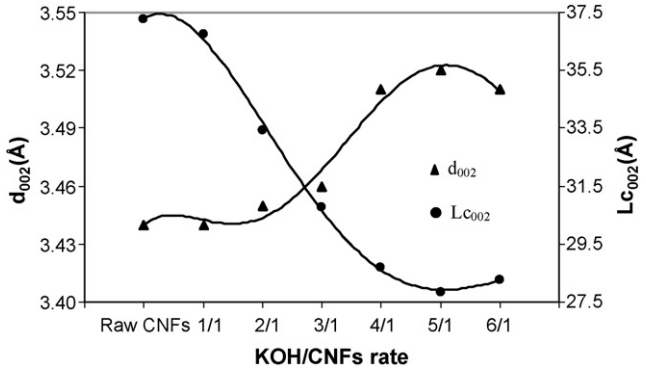

Fig. 3. *Influence of the KOH/CNFs ratio*: variation of XRD parameters (Lc_{002} and d_{002}).

than raw CNFs or less activated CNFs. The results obtained are clearly in good agreement with XRD analysis data.

The graphitization degree can be quantified using the average interlayer spacing (d_{002}) and the average stacking height of carbon planes (Lc_{002}), which have been plotted against the KOH/CNFs mass ratio (Fig. 3). The mean *n*umber of graphene *p*lanes in the crystallites (npg), calculated using the formula npg = Lc/d_{002}, are given in Table 1. It can be observed that d_{002} values increased and Lc_{002} values decreased in the activated samples when the KOH/CNFs mass ratio was increased, reaching a maximum and minimum, respec-

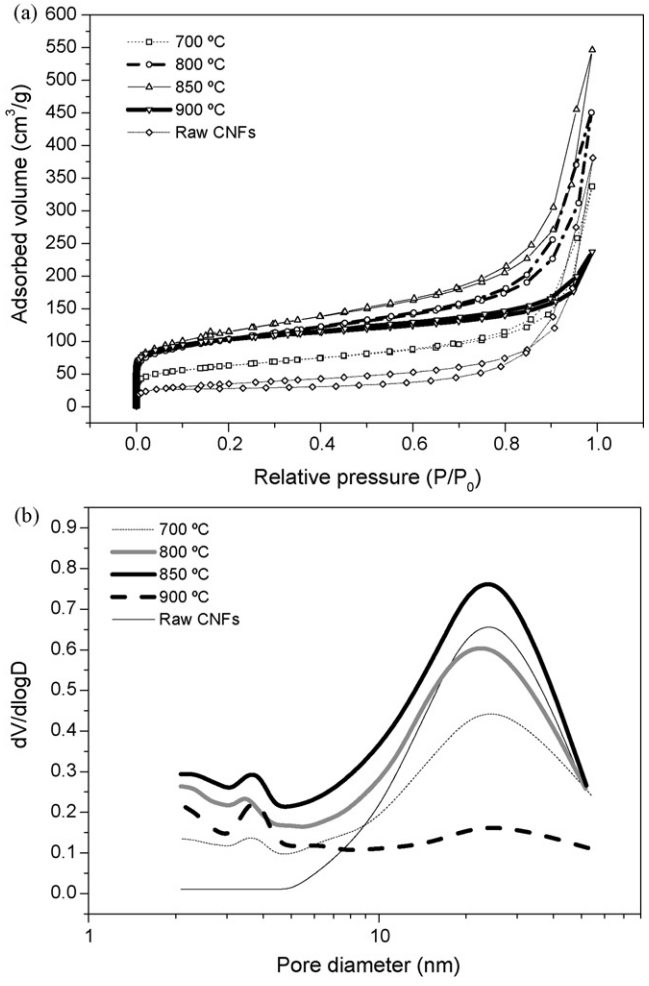

Fig. 4. *Influence of the activation temperature*: (a) N_2 adsorption–desorption isotherms and (b) mesopore size distribution.

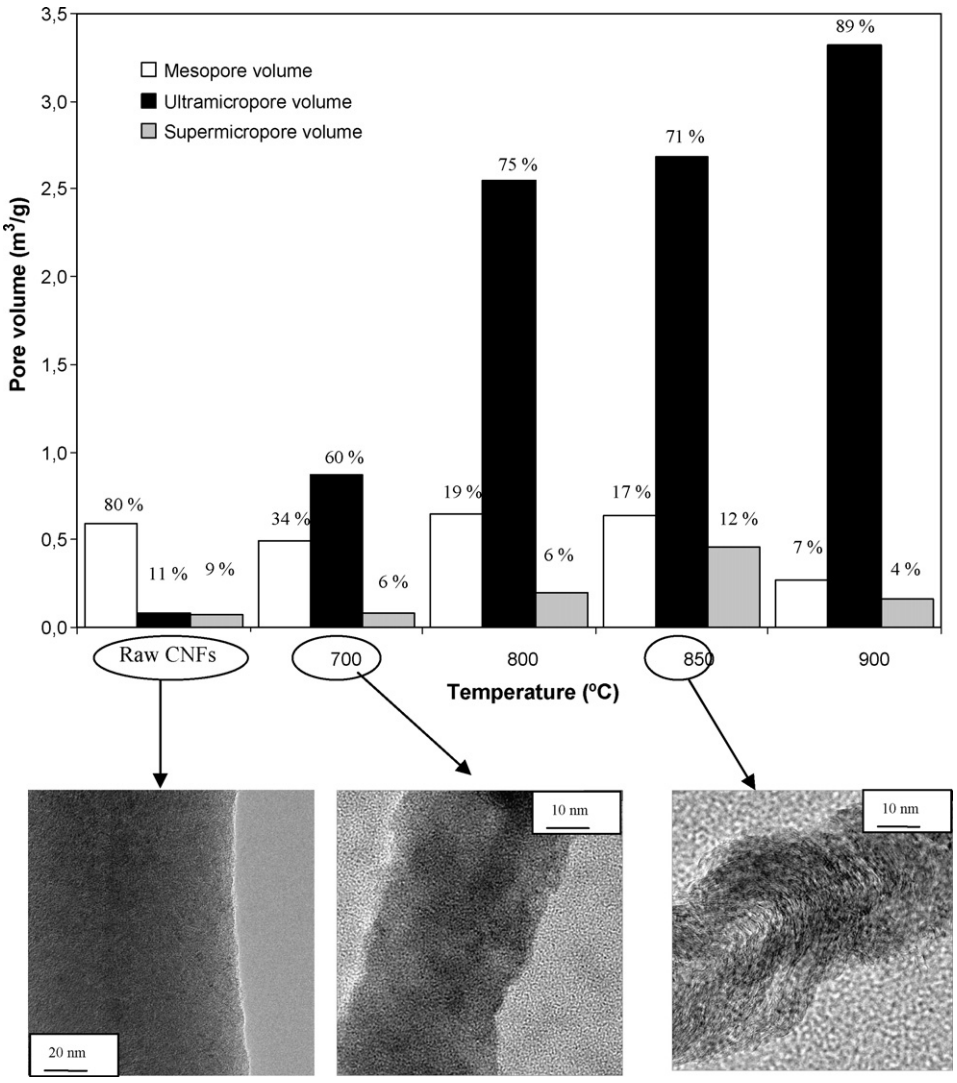

Fig. 5. *Influence of the activation temperature*: proportion of ultramicropores, supermicropores and mesopores. Representative TEM images.

tively, for a KOH/CNFs ratio of 5/1, which in turn led to a maximum BET surface area value. The npg values decreased from 10.8 for the raw CNFs to 7.9 for the CNFs activated using a KOH/CNFs mass ratio value of 5/1. These values are relatively high when compared with those reported for conventional activated carbon or activated carbon fibers, indicating that the graphitic nature of the raw CNFs was retained in the activated samples [12].

Finally, according to the mass balance shown in Table 1, raw CNFs were composed of carbon, hydrogen and oxygen, in a relative molar proportion of 92%, 5.5% and 2.5%. After the activation process, the carbon content decreased [30] and the hydrogen content remained approximately constant, whereas the oxygen content increased (C/O ratio decreased markedly in CNFs with the activation degree) [16].

3.2. Influence of the activation temperature

The activation temperature was varied from 700 to 900 °C while keeping the rest of the parameters constant (KOH/CNFs mass ratio, activation time and helium flow rate were 5/1, 3 h and 500 mL min^{-1}, respectively).

Nitrogen isotherms measured at 77 K on raw CNFs and CNFs activated at different temperatures are shown in Fig. 4a. As before, all isotherms correspond to a mixture of types I–IV, indicating that both micropores and mesopores were generated. The enlarged hysteresis loop space between the adsorption/desorption isotherms for the activated samples indicates the presence of a large amount of mesopores. On the other hand, the line climbs steeply in the area of low relative pressure, indicating that plenty of micropores were present [26]. As can be seen from the isotherms, a gradual increase in the amount of adsorbed N_2 with the activation temperature took place at temperatures lower than or equal to 850 °C, indicating a higher activation degree. However, as the temperature was increased to 900 °C amount of adsorbed N_2 decreased as a consequence of the lack of mesoporosity ($P/P_0 > 0.2$) in the resulting material.

The textural characteristics of the CNFs activated in this study are given in Table 1. As expected, the total BET surface area and micropore volume increased with activation temperature up to 850 °C, mainly due to the generation of micropores, and then decreased again. Consequently, the mesopore volume remained approximately constant at temperatures below 850 °C and then decreased at higher temperatures. As expected, the carbon yield was inversely proportional to the surface area due to the elimination of the most reactive carbon atoms after the activation process.

The proportions of ultramicropores, supermicropores and mesopores in the activated samples are shown in Fig. 5. It can be observed that the amount of ultramicropores increased when the

activation temperature was increased. Nevertheless, the amount of mesopores remained constant or increased slightly up to 850 °C and then decreased at higher temperatures. These results can be confirmed from the mesopore size distribution calculated from desorption branch by the BJH method (Fig. 4b). The population of micropores was enhanced even when the temperature was increased to 900 °C in contrast with the situation observed for the population of mesopores, which decreased significantly [26].

In summary, the activation temperature is a very important parameter in controlling the porosity of CNFs. Activated samples with a high level of micropores (mainly ultramicropores) can be obtained at high temperatures (900 °C), but if a high proportion of mesopores is also required, it would be necessary to activate the raw CNFs at lower temperatures (around 800–850 °C). The activation temperature used will depend on the end use of the activated CNFs (catalytic support, hydrogen storage, etc.).

In order to explain the results obtained, it is necessary to take into consideration the fact that K in the metal form must be formed during the activation reaction. Although this metal can be removed from the carbon matrix by evaporation (boiling point of K: 762 °C), a proportion of it could also be intercalated, which would produce a pore opening in the parent CNFs since some graphitic structures would be destroyed and micropores and mesopores would be generated [26]. A strong interaction between the potassium and CNFs will clearly led to the generation of new mesopores while a mild interaction will induce only the generation of micropores (in some cases at the expense of the original mesopores). In conclusion, the generation of micropores would also require a weak interaction between the activating agent and the CNFs. Moreover, this interaction would be easily improved on increasing the temperature. Nevertheless, if the reaction temperature exceeded a certain limit, no new mesopores would not be generated; in fact, they could even disappear through the interaction with the activating agent (K) generating some new micropores [26]. Mesopore development is usually associated with exfoliation of graphite layers, which can be confirmed by TEM (Fig. 5). At 850 °C it was possible to observe a CNF structure consisting of expanded graphite with zones of low density. Moreover, whereas the TEM image of raw CNFs showed a relatively smooth surface, activated CNFs (both weak and strong interactions) showed many defects along the surface.

The two main XRD analysis parameters (d_{002} and Lc_{002}) and the related npg parameter for raw CNFs and activated CNFs were evaluated (Table 1). As expected, npg values decreased with the activation temperature (Lc_{002} values decreased and d_{002} values increased in the activated samples with increasing temperature), passing through a minimum at 850 °C. Therefore, it can be clearly seen that the disorder of the carbon structures (d_{002}) increased and the crystallite size (Lc_{002}) decreased after the activation process, with maximum and minimum values, respectively, at 850 °C (maximum value of BET surface area). These results were also confirmed by means of TPO analyses (Table 1).

Finally, the chemical composition of the raw and activated CNFs according to elemental analysis is given in Table 1. The carbon content of CNFs decreased and the oxygen content increased after heat treatment [30], reaching a minimum or maximum at 850 °C and then increasing or decreasing again, respectively.

3.3. Effect of activation time

In order to examine the effect of activation time on the activated CNFs, this parameter was varied from 1 to 4 h while keeping the other parameters constant.

The influence of the activation time on the N_2 adsorption isotherms is shown in Fig. 6a. The differences between CNFs activated during 1 h and the other materials were significant in both the low and high relative pressure zones. However, the differences

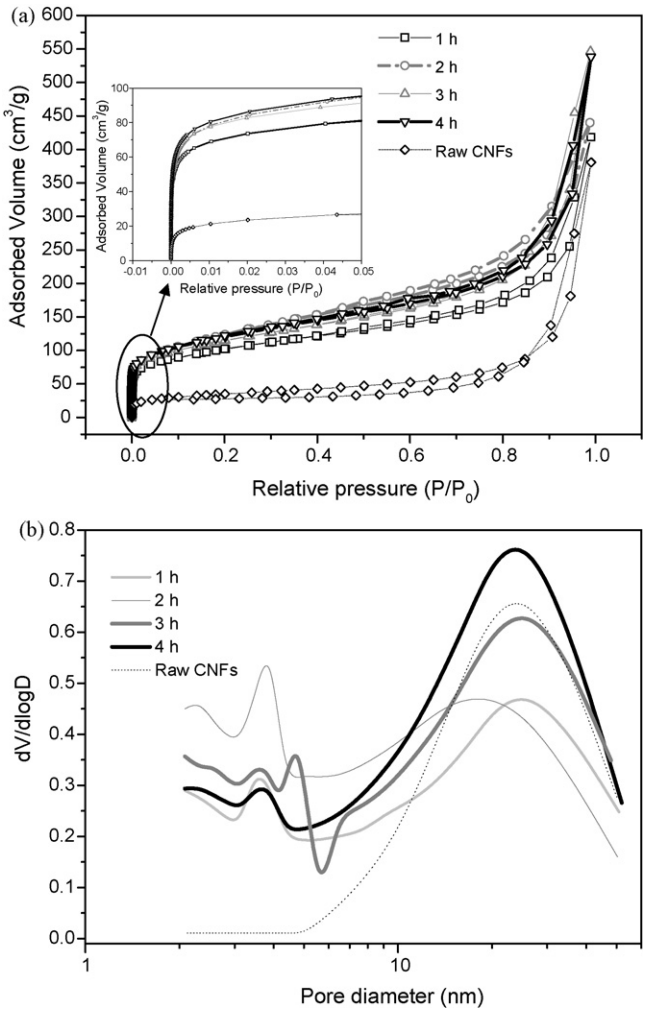

Fig. 6. *Influence of the activation time*: (a) N_2 adsorption–desorption isotherms and (b) mesopore size distribution.

in the N_2 adsorption capacity between CNFs activated for 2, 3 or 4 h were very small, principally in the low pressure zone (see the insert in Fig. 6a). These results were also confirmed by the textural parameters shown in Table 1. On the other hand, the mesoporosity of the activated CNFs (expressed as dV/dlog D in Fig. 6b) corresponded to pore sizes in the range 2–10 nm. Mesopores with higher pore sizes were only formed when the reaction time was longer than 3 h. All activated samples showed a strong peak located at around 22 nm, which was also observed for the raw CNFs, indicating that their tubular structure was maintained to some extent after activation [26].

The proportions of ultramicropores, supermicropores and mesopores in the activated samples are shown in Fig. 7. It can be seen that, in all cases, the inherent mesoporosity of the parent CNFs decreased as a percentage during the activation process due to the creation of micropores (mainly ultramicropores). In other words, although some mesopores were generated, their percentage with respect to the total was reduced. On that basis, micropores were formed initially during the activation process and then widened to give larger micropores and also mesopores. Thus, the amount of micropores increased with increasing activation times, reaching a maximum after 3 h of reaction. However, when the activation time was 4 h the amount and percentage of ultramicropores and supermicropores decreased as the mesopore levels increased. These results can be explained by considering the total consumption of the activating agent. Thus, it is possible that KOH was totally

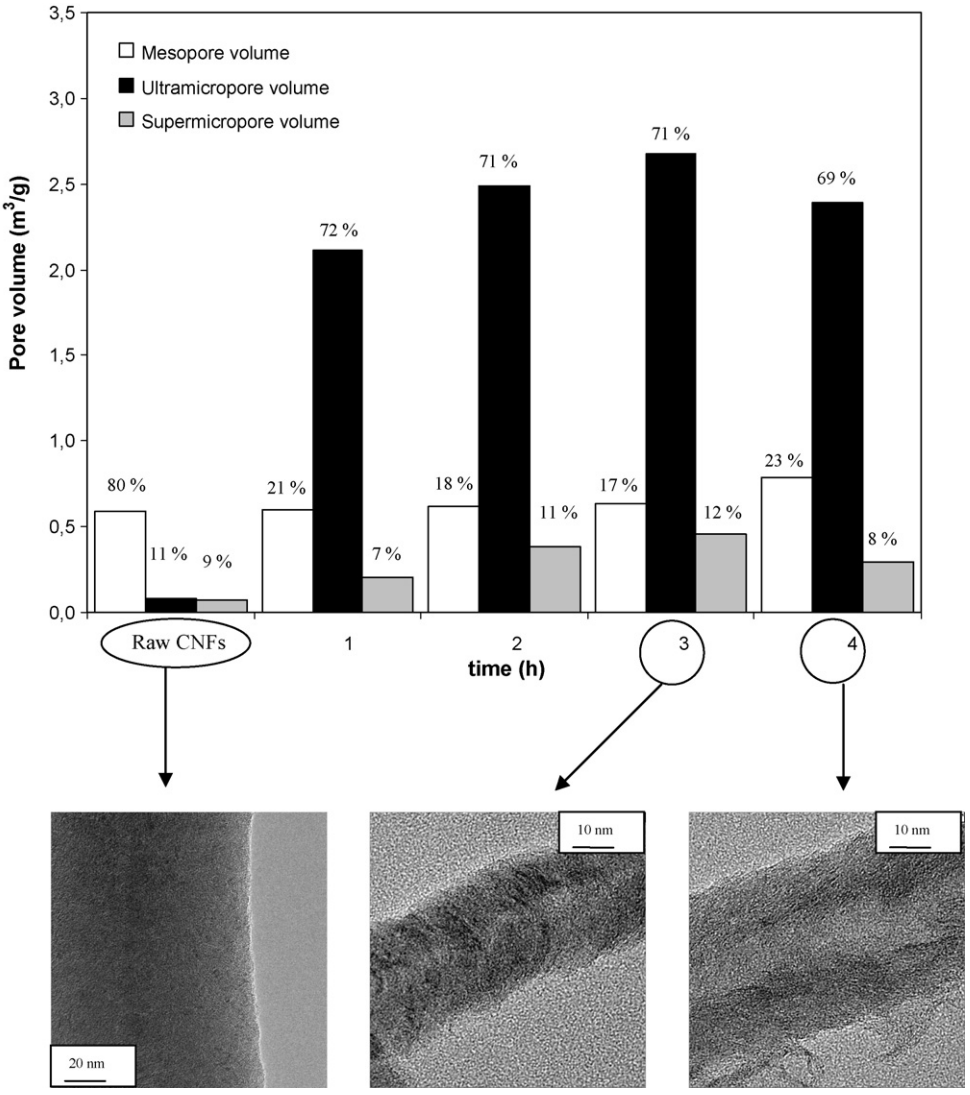

Fig. 7. *Influence of the activation time*: proportion of ultramicropores, supermicropores and mesopores. Representative TEM images.

exhausted after 3 h of reaction (maximum values of the textural parameters). After that time, reforming reactions could occur in the activated CNFs as a consequence of the high temperatures used. Thus, some micropores widened to larger mesopores and this would decrease the surface area and micropore volume but increase the mesopore volume [31]. The TEM images shown in Fig. 7 reveal the higher degree of expanded graphite layers present in CNFs activated during 4 h (a hollow core with low graphite density is clearly visible).

As noted above, the yield of activated CNFs decreased as the porosity of the material was increased (Table 1). Once again, the carbon content was lower and the oxygen content was higher with higher porosity structure development. On the other hand, the hydrogen content remained approximately constant in all activated samples.

Finally, the influence of the activation time on npg values can be seen from the results in Table 1. The graphitization degree decreased with the porosity development. Nevertheless, the changes in npg values were not particularly marked (if compared with those obtained in the study of the influence of other reaction parameters), indicating that the reaction time is not a very important parameter in controlling the crystallinity of CNFs after the activation process.

3.4. Effect of helium flow rate

In the activation process, nitrogen is usually used as a protection gas [6,14,31,32]. However, in a previous publication we reported that He works better than N_2 and, at the same time, has a significant effect on the porosity development [17]. Thus, the He flow rate varied in the range 150–1000 mL min^{-1} with the values of the other parameters kept constant.

The nitrogen adsorption isotherms at 77 K for the activated CNFs using different He flow rates are shown in Fig. 8 and the results of the porous texture analysis for these samples are given in Table 1. It can be seen that increasing He flow rates favoured the development of porosity, including both micropores and mesopores, until a value of 700 mL min^{-1} was reached. A further increase in the He flow rate led to a decrease in the porosity development [31]. As mentioned before, an increase in the N_2 adsorption capacity was observed in all isotherm regions (both in the zone of low and high relative pressure) indicating that all types of pores were developed during the activation process. This fact can also be confirmed from the information in Table 1 (the values of the total micropore and mesopore volume) and Fig. 9, which shows a plot of the proportions of ultramicropores, supermicropores and mesopores.

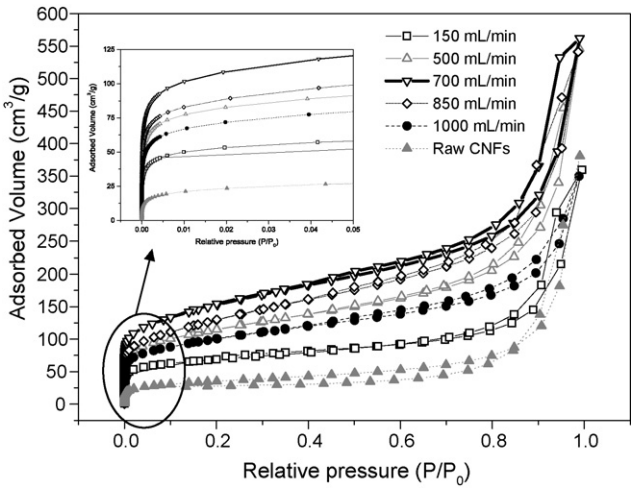

Fig. 8. *Influence of He flow rate*: N_2 adsorption–desorption isotherms.

To explain the results obtained it is necessary to consider the removal of gases evolved during the activation process. Thus, a faster removal of gases favours the porosity development and this occurred at higher flow rates. According to Raymundo-Piñero et al. [19], the activation mechanism could be as follows: the reduction of hydroxide by carbon would lead to H_2, K and carbonates, a simultaneous possible reaction between KOH and C could occur although, depending on the temperature range considered, this may not be thermodynamically feasible [11]; the CO_2 produced in the last reaction could also react with the hydroxide [11]:

$$6KOH + 2C \rightleftarrows 2K + 3H_2 + 2K_2CO_3 \quad (1)$$

$$4KOH + C \rightleftarrows 4K + CO_2 + 2H_2O \quad (2)$$

$$4KOH + 2CO_2 \rightleftarrows 2K_2CO_3 + 2H_2O \quad (3)$$

As observed, K could be formed during the pyrolysis process and this could be continuously removed from reaction site (due to the He flow) once its role has been fulfilled. Once K is removed, the equilibrium of reaction (1) would be displaced to the production of further K, thus increasing the degree of reaction between CNFs and KOH [6]. On the other hand, H_2O formed during the pyrolysis reaction at high temperature would have the ability to penetrate into the solid material and aid both desorption and the efficient removal of volatile products from the solid. The water vapour is also a reactive agent and could react with pyrolysis products, stabilising the radicals obtained in the thermal decomposition and thus increasing the yield of volatiles [33]. As a result, the removal of H_2O (v) would work against the activation, while the removal of CO, CO_2 and H_2

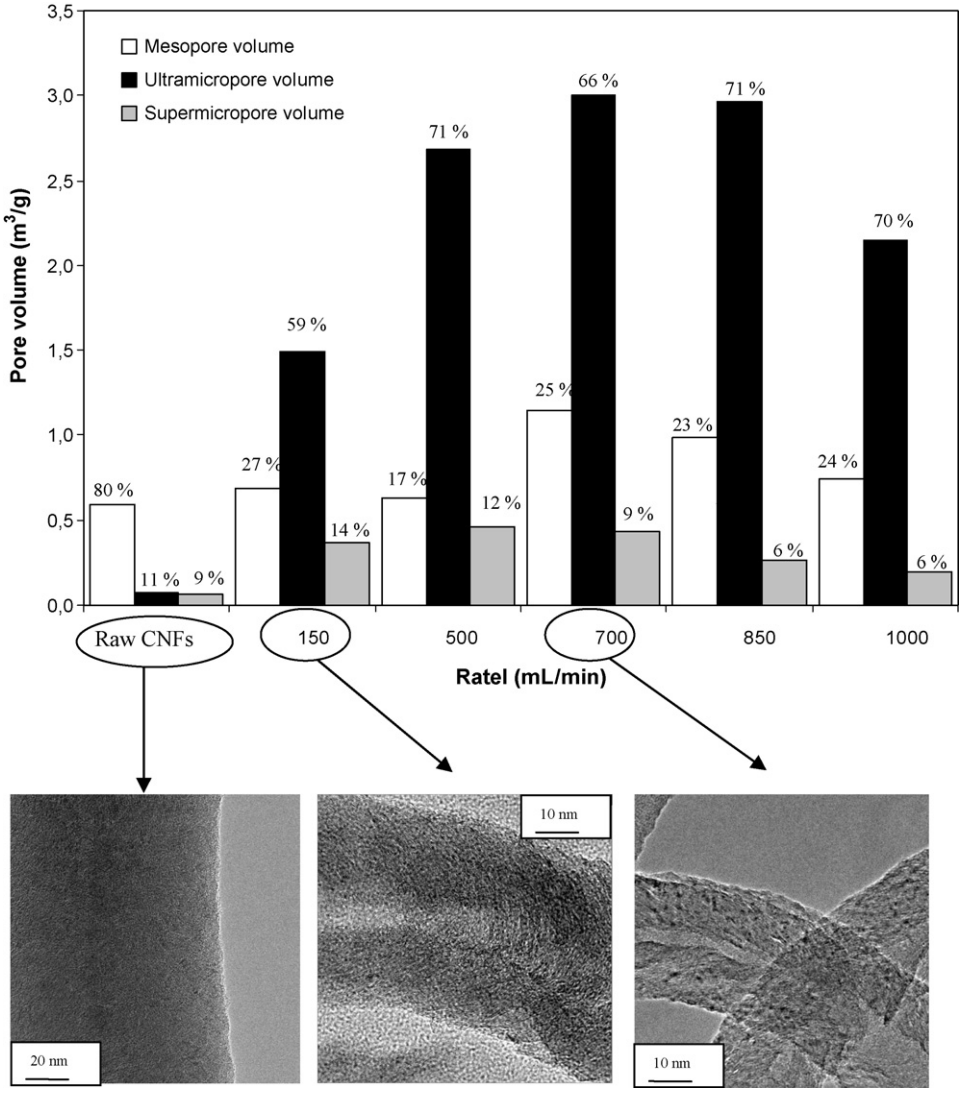

Fig. 9. *Influence of He flow rate*: proportion of ultramicropores, supermicropores and mesopores. Representative TEM images.

would favour the activation process. Therefore, a balance between these two removal processes would exist: a He flow rate that is too high could remove from the reaction site a large amount of H_2O and this would be detrimental to the porous properties of CNFs; a low He flow rate would probably not remove sufficient amounts of CO, CO_2, which would be in detrimental to the activation [31,32].

The influence of the He flow rate on the average interlayer spacing (d_{002}) and the average stacking height of carbon planes (Lc_{002}) expressed as npg values are shown in Table 1. Once again, it was noted that the higher the activation degree the more marked the change in the value of this parameter. The range of npg values in this study (6.7–10.8) was higher than that obtained in the study of other parameters, thus clearly establishing that the He flow rate is one of the most important parameters in controlling the crystallinity of the CNFs after an activation process. These results are in good agreement with those obtained by TPO analyses.

Finally, the elemental composition (see Table 1) confirmed that after activation the hydrogen content remained approximately constant, that the carbon content decreased and the oxygen content increased. In this study, the range of variation in the elemental composition was also higher when compared with other values in this work.

4. Conclusions

This work described here focused on the study of the influence of the activation conditions on the structure of herringbone carbon nanofibers using KOH chemical activation process.

The structural properties of activated CNFs were found to depend on the conditions used during activation process. In this way, it possible to obtain CNFs with higher levels of mesopores or higher levels of micropores depending on the end use of the material. The highest surface area and micropore volume were obtained using KOH/CNFs ratio = 5/1, activation temperature = 850 °C, activation time = 3 h and a He flow rate = 700 mL min^{-1}. Some mesopores were also created due to the strong interaction between CNFs and the activating agent. On the other hand, activation of the CNFs using a KOH/CNFs ratio = 5/1, activation temperature = 900 °C, activation time = 3 h and a He flow rate = 500 mL min^{-1} gave rise to the lowest mesopore volume.

In summary, depending on the final application of the activated materials, it is possible to control their pore structure by choosing appropriate activation conditions.

Acknowledgements

The authors gratefully acknowledge the financial support from Consejería de Ciencia y Tecnología de la Junta de Comunidades de Castilla-La Mancha (Projects PBI-05-038 and PCI 08-0020-1239).

References

[1] T.K. Baker, K. Laubernds, A. Wootsch, Z. Paal, Pt/graphite nanofiber catalyst in n-hexane test reaction, J. Catal. 193 (2000) 165.
[2] K. Lozano, E.V. Barrera, Nanofiber-reinforced thermoplastic composites. I. Thermoanalytical and mechanical analyses, J. Appl. Polym. Sci. 79 (2001) 125.
[3] C.A. Bessel, K. Laubernds, N.M. Rodriguez, R.T.K. Baker, Graphite nanofibers as an electrode for fuel cell applications, J. Phys. Chem. B 105 (2001) 1115.
[4] C. Park, R.T.K. Baker, Carbon deposition on iron–nickel during interaction with ethylene–carbon monoxide–hydrogen mixtures, J. Catal. 190 (2000) 104.
[5] M. Marella, M. Tomaselli, Synthesis of carbon nanofibers and measurements of hydrogen storage, Carbon 44 (2006) 1404.
[6] D. Lozano-Castelló, M.A. Lillo-Ródenas, D. Cazorla-Amorós, A. Linares-Solano, Preparation of activated carbons from Spanish anthracite. I. Activation by KOH, Carbon 39 (2001) 741.
[7] C. Merino, P. Soto, E. Vilaplana-Ortego, J.M. Gomez de Salazar, F. Pico, J.M. Rojo, Carbon nanofibres and activated carbon nanofibres as electrodes in supercapacitors, Carbon 43 (2005) 551.
[8] A. De Lucas, A. Garrido, P. Sánchez, A. Romero, J.L. Valverde, Growth of carbon nanofibers from Ni/Y zeolite based catalysts: effects of Ni introduction method, reaction temperature, and reaction gas composition, Ind. Eng. Chem. Res. 44 (2005) 8225.
[9] M.J.B. Evans, E. Halliop, J.A.F. MacDonald, The production of chemically-activated carbon, Carbon 37 (1999) 269.
[10] M. Wu, Q. Zha, J. Qui, Y. Guo, H. Shang, A. Yuan, Preparation and characterization of porous carbons from PAN-based preoxidized cloth by KOH activation, Carbon 42 (2004) 205.
[11] M.A. Lillo-Ródenas, D. Cazorla-Amorós, A. Linares-Solano, Understanding chemical reactions between carbons and NaOH and KOH: an insight into the chemical activation mechanism, Carbon 41 (2003) 267.
[12] D. Luxembourg, X. Py, A. Didion, R. Gadiou, C. Vix-Guterl, G. Flamant, Chemical activations of herringbone-type nanofibers, Micropor. Mesopor. Mater. 98 (2007) 123.
[13] S. Yoon, S. Lim, Y. Song, Y. Ota, W. Qiao, A. Tanaka, I. Mochida, KOH activation of carbon nanofibers, Carbon 42 (2004) 1723.
[14] M.A. Lillo-Ródenas, D. Lozano-Castelló, D. Cazorla-Amorós, A. Linares-Solano, Preparation of activated carbons from Spanish anthracite. II. Activation by NaOH, Carbon 39 (2001) 751.
[15] J.A. Maciá-Agulló, B.C. Moore, D. Cazorla-Amorós, A. Linares-Solano, Influence of carbon fibres crystallinities on their chemical activation by KOH and NaOH, Micropor. Mesopor Mater. 101 (2007) 397.
[16] V. Jiménez, P. Sánchez, A. De Lucas, J.L. Valverde, A. Romero, Influence of the nature of the metal hydroxide in the porosity development of carbon nanofibers, J. Colloid Interface Sci. 336 (2009) 226.
[17] V. Jiménez, P. Sánchez, J.L. Valverde, A. Romero, Influence of the activating agent and the inert gas (type and flow) used in an activation process for the porosity development of carbon nanofibers, J. Colloid Interface Sci. 336 (2009) 712.
[18] Y.A. Zhu, Z.J. Sui, T.J. Zhao, Y.C. Dai, Z.M. Cheng, W.K. Yuan, Modeling of fishbone-type carbon nanofibers: a theoretical study, Carbon 43 (2005) 635.
[19] E. Raymundo-Piñero, P. Azaïs, T. Cacciaguera, D. Cazorla-Amorós, A. Linares-Solano, F. Béguin, KOH and NaOH activation mechanisms of multiwalled carbon nanotubes with different structural organisation, Carbon 43 (2005) 786.
[20] M.A. Lillo-Rodenas, J. Juan-Juan, D. Cazorla-Amorós, A. Linares-Solano, About reactions occurring during chemical activation with hydroxides, Carbon 42 (2004) 1371.
[21] J. Diaz-Teran, D.M. Nevskaia, J.L.G. Fierro, A.J. Lopez-peinado, A. Jerez, Study of chemical activation process of a lignocellulosic material with KOH by XPS and XRD, Micropor. Mesopor. Mater. 60 (2003) 173.
[22] R. Xue, Z. Shen, Formation of graphite-potassium intercalation compounds during activation of MCMB with KOH, Carbon 41 (2003) 1862.
[23] S. Mitani, S.I. Lee, K. Saito, S.H. Yoon, Y. Korai, I. Mochida, Activation of coal tar derived needle coke with K_2CO_3 into an active carbon of low surface area and its performance as unique electrode of electric double-layer capacitor, Carbon 43 (2005) 2960.
[24] A. De Lucas, P.B. García, A. Garrido, A. Romero, J.L. Valverde, Catalytic synthesis of carbon nanofibers with different graphene plane alignments using Ni deposited on iron pillared clays, Appl. Catal. B 301 (2006) 123.
[25] A. Romero, A. Garrido, A. Nieto-Márquez, A.R. De la Osa, A. De Lucas, J.L. Valverde, The influence of operating conditions on the growth of carbon nanofibers on carbon nanofiber-supported nickel catalysts, Appl. Catal. A 319 (2007) 246.
[26] J.J. Niu, J.N. Wang, Effect of temperature on chemical activation of carbon nanotubes, Solid State Sci. 10 (2008) 1189.
[27] M. Abe, H. Kataura, H. Kira, T. Kodama, S. Suzuki, Y. Achiva, K.I. Kato, M. Takata, A. Fujiwara, K. Matsuda, Y. Maniwa, Structural transformation from single-wall to double-wall carbon nanotube bundles, Phys. Rev. B 68 (4) (2003) 414051.
[28] P. Trucano, R. Chen, Structure of graphite by neutron diffraction, Nature 258 (5531) (1975) 136.
[29] H. Lipson, A.R. Stokes, The structure of graphite, Proc. R. Soc. Lond. A 181 (984) (1942) 101.
[30] R.L. Tseng, Mesopore control of high surface area NaOH-activated carbon, J. Colloid Interface Sci. 303 (2006) 494.
[31] Q. Jiang, Y. Zhao, Effects of activation conditions on BET specific surface area of activated carbon nanotubes, Micropor. Mesopor. Mater. 76 (2004) 215.
[32] R. Azargohar, A.K. Dalai, Steam and KOH activation of biochar: experimental and modeling studies, Micropor. Mesopor. Mater. 110 (2008) 413.
[33] V. Minkova, M. Razvigorova, E. Bjornbom, R. Zanzi, T. Budinova, N. Petrov, Effect of water vapour and biomass nature on the yield and quality of the pyrolysis products from biomass, Fuel Process. Technol. 70 (2001) 53.